

Prototype demonstration of the broadband anti-reflection coating on sapphire using a sub-wavelength structure

T. Matsumura¹, R. Takaku^{2,3}, S. Hanany⁴, H. Imada^{5,6}, H. Ishino⁷, N. Katayama¹, Y. Kobayashi⁸, K. Komatsu⁷, K. Konishi⁹, M. Kuwata-Gonokami³, S. Nakamura², H. Sakurai³, Y. Sakurai¹, Q. Wen⁴, K. Young⁴, J. Yumoto^{3,9}

¹Kavli Institute for The Physics and Mathematics of The Universe (WPI), The University of Tokyo, Kashiwa, 277-8583, Japan

²Yokohama National University, Yokohama, 240-8501, Japan

³Department of Physics, The University of Tokyo, 113-0033, Japan

⁴The University of Minnesota, Twin Cities, MN 55455 USA

⁵Institute of Space and Astronautical Science (ISAS), Japan Aerospace Exploration Agency (JAXA), Sagami-hara, 252-5210, Japan

⁶Laboratoire de l'Accélérateur Linéaire, Université Paris-Sud, CNRS/IN2P3, Université Paris-Saclay, Université Paris-Sud, Bâtiment 200, 91898 Orsay, France

⁷Okayama University, Okayama, 700-8530, Japan

⁸The Institute for Solid State Physics, The University of Tokyo, Tokyo, 277-0882, Japan

⁹Institute for Photon Science and Technology, The University of Tokyo, Tokyo, 113-0033, Japan

*Contact: tomotake.matsumura@ipmu.jp

Abstract—We report the development of the broadband anti-reflection (AR) coating on sapphire using a sub-wavelength structure for a cosmic microwave background (CMB) polarization experiment. One of the challenges in the CMB polarization experiment is to disentangle the sources of the polarized emission among the CMB and the galactic emissions from our Galaxy. This leads a need of a cryogenically compatible broadband AR coating on a millimeter wave optical element used in a CMB telescope. We design and fabricate the AR sub-wavelength structure using a laser machining on a sapphire plate, which is a commonly used material as a half-wave plate at millimeter wavelength. We fabricate a prototype sample and evaluate the transmittance of an SWS AR sapphire for the fractional bandwidth of about 1.5. We show the agreement between the measured transmittance and the prediction based on the fabricated shape. The projected transmittance based on the measurement achieves above 90% above 50 GHz. We finally discuss the room of the improvement and the applicability for this technology for a future CMB polarization experiment.

I. INTRODUCTION

The measurement of the cosmic microwave background (CMB) has played an important role in the modern cosmology. The recent rapid progress of the technological developments in the CMB experiment brings the community to the next target, testing the hypothesis of the cosmic inflation experimentally. Today, there is a strong enhancement between the scientific motivation and the technological development [1,2].

One of the major challenges in the CMB polarization experiment is to make a distinction between the CMB and the

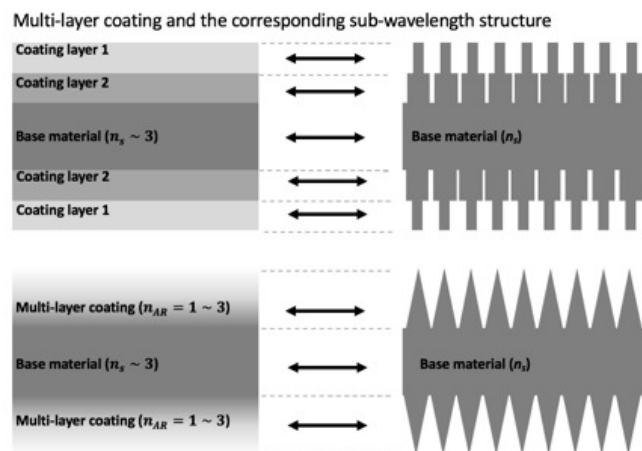


Figure 1 A sketch to show the correspondence between the multi-layer based AR coating and the SWS based AR strategy.

galactic polarized emissions from our own Galaxy. The standard method is to separate the different sources of the emission by relying on the difference of the spectral shape by observing a broad bandwidth. As a result, the recent CMB polarization telescope is in need of covering the broadband frequency coverage, ideally speaking from a centimeter wavelength to sub-millimeter wavelength.

One of the limitations in a broadband observation comes from the available bandwidth of the anti-reflection (AR) coating on an optical element in a CMB telescope. Typically, a CMB telescope employs a filter, a lens, and a half-wave

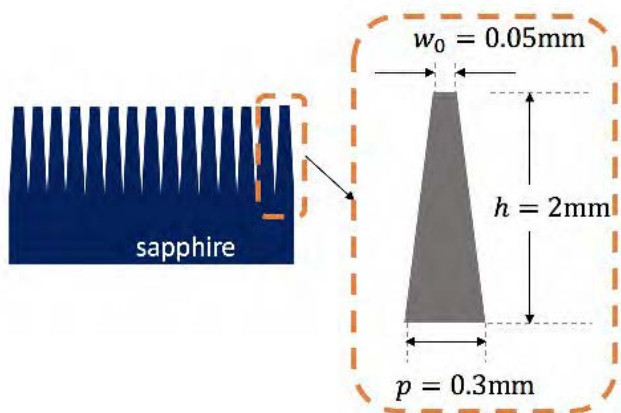


Figure 2 The sketch shows the parameterization of the pyramidal structure using three parameters.

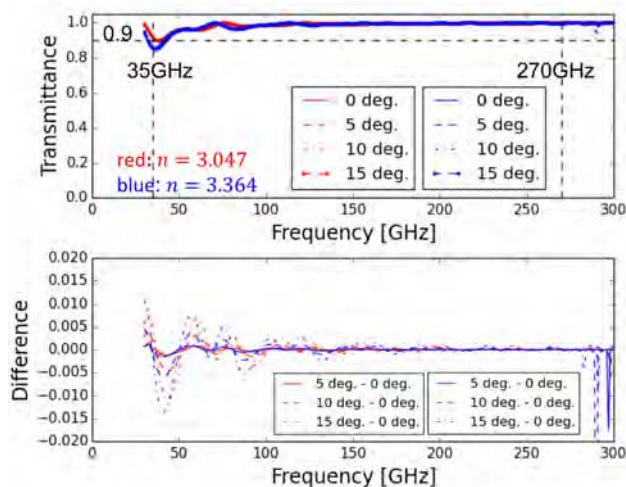


Figure 3 Top panel: The transmittance as a function of the frequency for the geometry in Figure 2. Bottom panel: The differential transmittance of the non-normal incident radiation with respect to the normal incident radiation. The thickness of the sapphire substrate, not including the AR layer, is assumed to be 1 mm in this simulation.

plate. All of these are a transmissive optical element, and thus it suffers from reflection without any AR coating. The typical materials, e.g. silicon, alumina, sapphire, have the index of refraction of about 3, and the resultant reflection without any AR coating is the reflectance of about 50%. Therefore, it is essential to apply a proper AR coating in order to maintain enough throughput of a telescope.

For a narrow bandwidth application, the standard technique to achieve the AR coating is to employ a thin dielectric layer with the index of refraction, $\sqrt{n_s}$. The valuable, n_s , is the index of refraction of the substrate on which we apply the AR coating. The thickness of the thin dielectric layer is $d_{AR} = \lambda_c/4\sqrt{n_s}$, where λ_c is the wavelength to minimize the reflection. This condition achieves a perfect transmission at a single frequency, $\nu_c = c/\lambda_c$, and its harmonics. Transmittance drops when the frequency of an interest departs away from the targeted frequency, ν_c . It achieves the fractional bandwidth of $\sim 30\%$ for above 90% of transmittance [3].

For a broadband coverage, the conventional method is to employ a multi-layer based AR coating. In recent years, there has been a tremendous development effort by using this multi-layer based AR coating on a flat disk and/or a curved lens [4-6]. The multi-layer based AR coating has two potential problems. One limitation is in its availability of materials for the various indices of refractions with a low dielectric loss. Another limitation is a mismatch of the coefficient of the thermal contraction among the materials. The coated layers potentially peel off the layers and eventually lead to the crack of each layer. In the worst case, it breaks the substrate itself.

In order to overcome these effects, another approach has been taken using sub-wavelength structure (SWS) based AR. The SWS, also known as a moth's eye structure, can provide the effective index of refraction between vacuum and a substrate. The desired index can be obtained by tuning the volume fraction between vacuum and the substrate in a unit volume as shown in Figure 1. The direct machining in the optical material can mitigate any issues originated from the differential thermal contraction. This also eliminates the search of a material that matches with a proper index of refraction and low loss.

Multiple methods have been explored to fabricate the SWS, dicing saw, etching, and laser machining [7-12]. In this paper, we address the laser machining approach on a sapphire plate, which is a typical material for a half-wave plate material at millimeter wavelength. The development is aimed to achieve the transmittance above 90% for the frequency range between 35 and 270 GHz. This bandwidth corresponds to the fractional bandwidth of 1.5, which has never been demonstrated.

This work is motivated by the technological development program, which is driven by the requirement from the next generation CMB satellite proposal, LiteBIRD [13,14]. It is a candidate mission proposal for a JAXA/ISAS strategic large class mission category and it is in a conceptual study phase. One of the telescopes of LiteBIRD is designed to cover the frequency range from 35 GHz to 161 GHz and possibly 270 GHz. One of the mission instruments for LiteBIRD is a half-wave plate polarization modulator using a sapphire. We require the design of the AR coating for a sapphire plate using a SWS method to cover 35 GHz to 161 GHz and we set the goal to cover up to 270 GHz.

In this paper, we report the design and the fabrication of the AR SWS on a sapphire plate. We also discuss the design trade-off, the feasibility and the implication of this technology toward a future CMB project.

II. SAMPLE PREPARATIONS

A. Design

We design the AR structure on a flat sapphire. The design goal is to cover the frequency range from 35 GHz to 270 GHz, which the LiteBIRD low frequency telescope was originally targeted to cover. We set the first requirement of this development to be transmittance of above 90% to cover this bandwidth. We design the SWS using a second order effective

medium theory (EMT) [15]. We start with a simple design, which is parameterized by the three parameters, a pitch, a height, and a top width as shown in the right of Figure 2. Generally speaking, the pitch determines the highest frequency which the AR structure can be functional below the diffraction limit. The combination of the height and the top width determines the AR performance at the low frequency end.

We verify the design performance without relying on the EMT, which is an approximated method. We compute predicted transmittance using a commercially available software, DiffractMod, which is based on Rigorous Coupled-Wave Analysis (RCWA) algorithm [16]. The parameters of a pitch of $p = 300 \mu\text{m}$, a height of $h = 2\text{mm}$, a top width of $w_0 = 50 \mu\text{m}$ on both sides of the A-cut sapphire result transmittance as shown in the top panel of Figure 3. In this simulation, we assume the thickness of the sapphire to be 1.0 mm. The pitch is determined to avoid the effect of the diffraction. We choose the pitch to be sufficiently finer than the frequency range of interest in order to avoid the effect of diffraction. The choice of the pitch, $p = \frac{c}{nv_c} = 300 \mu\text{m}$, results the diffraction limited frequency, ν_* , to be $\nu_* = 294 \text{ GHz}$ for $n = n_e$. Also, the index of the refraction is assumed to be $n_o = 3.047$ and $n_e = 3.364$, and the dielectric loss is neglected [17]. This first iteration of the design can achieve transmittance above 90% at the nearly full targeted bandwidth.

We also computed for the incident angle range in $\pm 5, 10, \text{ and } 15$ degrees. All the curves essentially overlap on the same curves. The bottom panel of Figure 3 shows the differential transmittance of the non-normal incident radiation with respect to the normal incident radiation. The RMS differential transmittance over the entire frequency range for 15-degree incident radiation is 0.3% for both the ordinary and extraordinary axes. The maximum reduction of transmittance is less than 1.5% from the transmittance of the normal incident radiation at the 40-50 GHz range.

B. Fabrication

We fabricate the SWS AR pattern on a C-cut sapphire by using a 3 W nano-second UV laser machine. We name this sample as the sample A. The top and middle panels of Figure 4 show the fabricated structure, which is observed by a confocal microscope. We have not done any optimization in machining time, and it took about 70 hours to fabricate this sample. There are a number of optimizations which we can address in the machining speed, but this is in progress and beyond the scope of this paper.

We choose a sapphire sample to be a C-cut crystal instead of an A-cut crystal. This is because we want to avoid the degeneracy between the performance of the AR structure and the effect due to the optic axis alignment with respect to the incident polarization angle. As a result, the interpretation is straightforward at the time of the experimental demonstration. The structure was made only one side for the demonstration purpose. The area of the machining is centered with the diameter of 21 mm to minimize the machining time.

The bottom of Figure 4 shows one dimensional slices of the image at two locations as shown with the dashed line in the middle panel of Figure 4. The measured shape parameters are

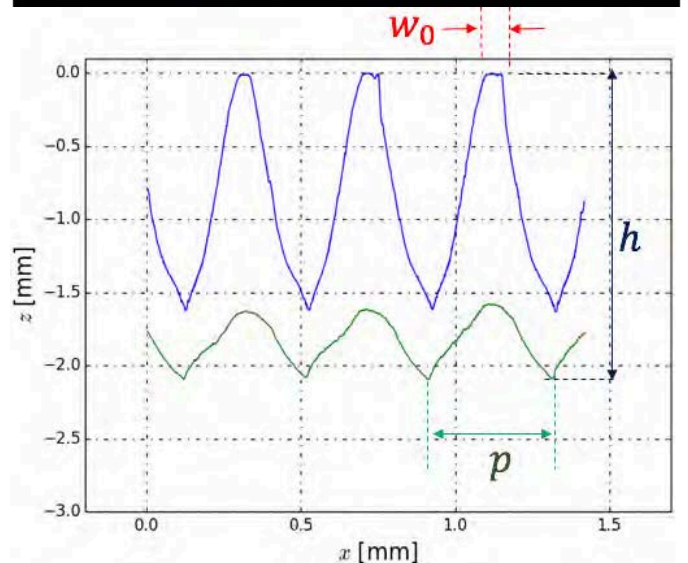
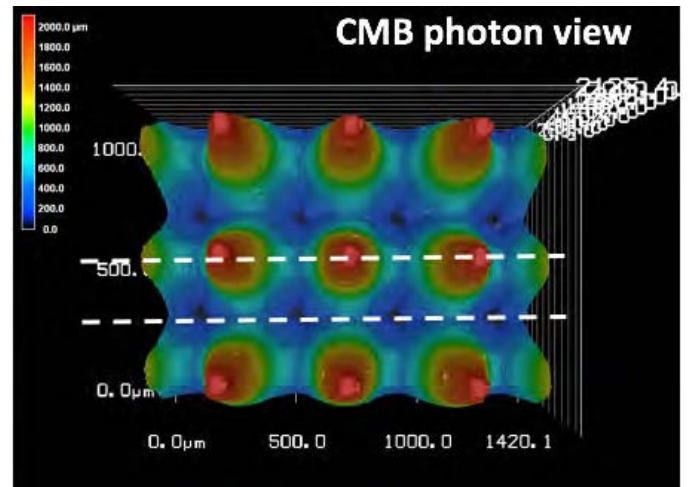
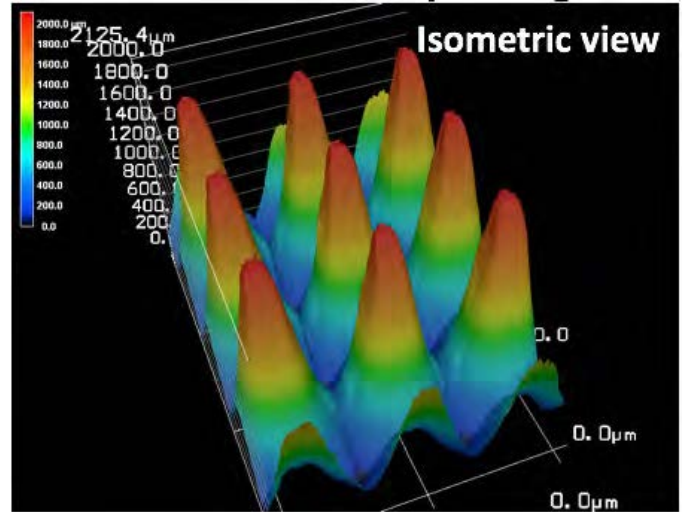


Figure 4 Top and middle: The confocal microscope images of the fabricated sample A. Bottom: The one dimensional sliced profile. The blue profile

corresponds to the slice which crosses the tip of the pyramid. The green profile corresponds to the slice which crosses the valley of the pyramid.

$w_0 = 51.3 \pm 7.2 \mu\text{m}$, $p = 398.7 \pm 6.1 \mu\text{m}$, and $h = 2105.0 \pm 21.3 \mu\text{m}$ while the designed values are $w_0 = 50 \mu\text{m}$, $p = 400 \mu\text{m}$, and $h = 2000 \mu\text{m}$. We picked the pitch

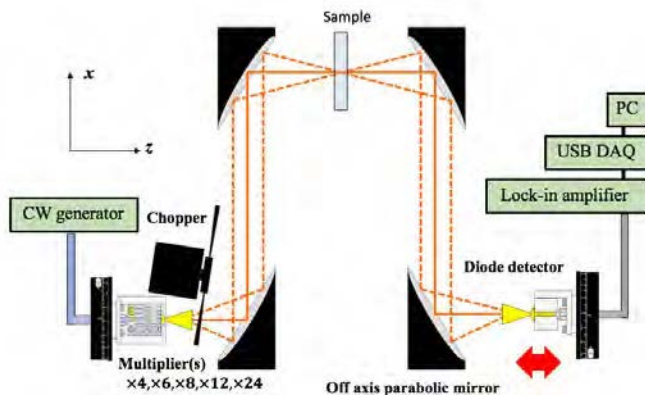


Figure 5 A sketch of the transmittance measurement set up at Kavli IPMU.

to be about 0.4 mm instead of 0.3 mm that is easier to machine due to the lower aspect ratio. The corresponding diffraction limited frequency is $\nu_*(n_o) = 246$ and $\nu_*(n_e) = 223$ GHz for the index of refraction n_e . The quoted errors are computed by the RMS fluctuation of the measured parameters from the 45 pyramids. We measure the shapes using the confocal microscope at 5 locations of the machined area, center, and 4 corners, and one location contains 9 pyramids.

This error can be interpreted as a measure of the repeatability of the SWS shape.

Due to the nature of a laser machining, the shape does not come out to be exactly the same as the designed shape. Thus, we evaluate the performance by both the millimeter wave transmittance experimentally and the simulation based prediction with the fabricated shape.

III. EXPERIMENTS

The measurement of transmittance is carried out by the millimeter-wave transmittance measurement setup at Kavli IPMU. Figure 5 shows the sketch of the measurement setup. We use a synthesizer to generate the electromagnetic wave frequency in range between 8 and 18 GHz. The source electromagnetic wave is propagated to a multiplier. We employ 6 different multipliers, Q-band ($\times 4$), V-band ($\times 4$), W-band ($\times 6$), F-band ($\times 8$), G-band ($\times 12$), Y-band ($\times 24$), to cover the frequency range from 35 to 265 GHz. Each transmittance measurement is done at a monochromatic frequency, and we sweep the frequency to cover the entire range. The frequency step of this sweep is chosen to be about 1 GHz to capture most of the spectral feature in transmittance. We normalize the transmitted power by dividing the measured power with the sample by the measured power without the sample. The sample is placed between the second and third mirrors, which is in focus. This is because we want to speed up the iteration of the development by preparing only a small sample, which saves a machining time. At the Gaussian waist, the spot diameter in the measurement bandwidth ranges from

2 mm to 15 mm. The Rayleigh length ranges from 20 mm to 158 mm, which is longer than the sample thickness of about 3 mm. The sample is tilted in the y - z plane by 5 degrees in order to minimize the standing wave along the chief ray. We also inserted attenuators to minimize this effect in the optical path.

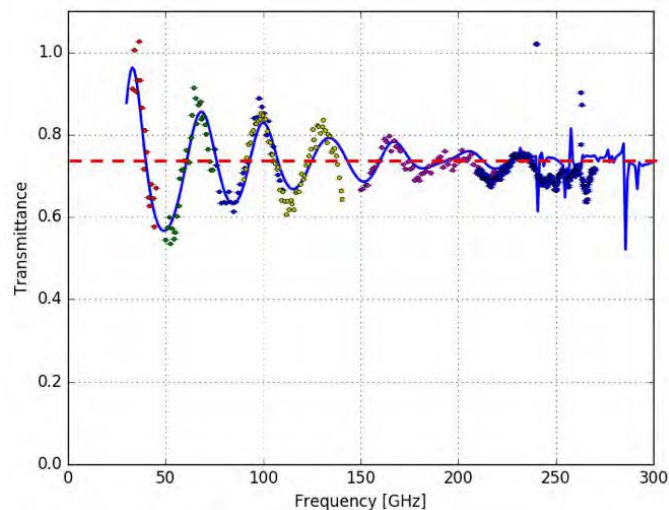


Figure 6 Fig. 6. The data points are the measured transmittance of the sample A and the solid line is the prediction based on the measured shape. The red dashed line is drawing at 0.74, which is the expected mean of transmittance from one side AR sample. The shape spikes in the prediction is due to the effect of diffraction.

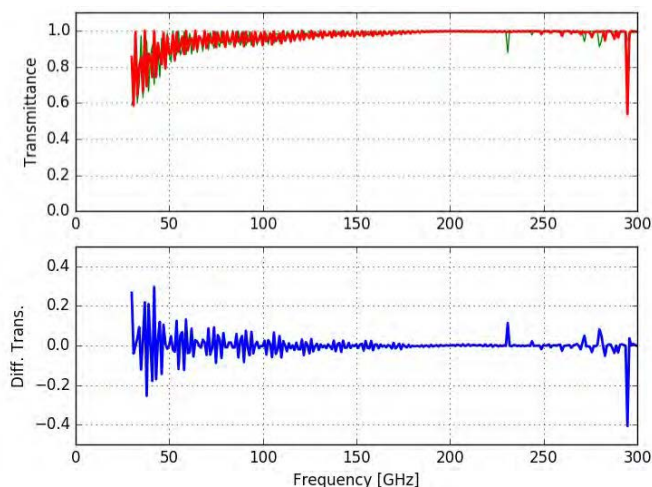


Figure 7 Top panel: The predicted transmittance given the fabricated geometry of the sample A using the DiffractMOD. The green and red curves are transmittance for the ordinary and extra-ordinary axes, T_o and T_e , respectively. Bottom panel: The differential transmittance between the ordinary and the extra-ordinary axes.

IV. RESULTS

The top panel of Figure 6 shows the measured transmittance as a function of frequency. The oscillatory features around the mean of 0.74 is due to the fact that the SWS AR is only applied on one side of the sapphire surface. A set of the colored data points corresponds to the same multiplier source. The predicted curve is over-plotted to the data points. The predicted curve is computed by the

DiffractMOD based on the measured shape from the confocal microscope. The accuracy of the calculating transmittance is below 10^{-4} . There is no free parameter to fit and the data and the prediction agree well. This also shows the validity of the predicted transmittance that is computed by the DiffractMOD given the measured shape data using a confocal microscope.

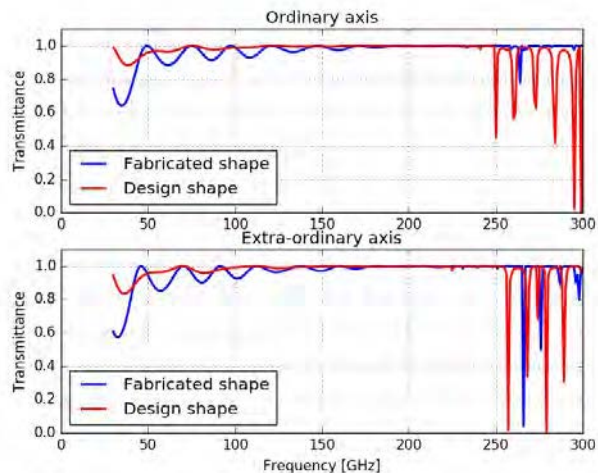


Figure 8 A comparison of the transmittance between the design shape and the fabricated shape.

The top panel of Figure 7 shows the prediction of transmittance when the fabricated AR structure is applied on both sides of the A-cut sapphire. The thickness is assumed to be 28.3 mm, which is assumed to have $3.14 \text{ mm} \times 9$ for use as an achromatic HWP [18]. Transmittance achieves above 90% for the frequency range above 70 GHz. When the band is averaged over 30% fractional bandwidth, the fast-oscillatory feature is smeared and averaged transmittance achieves above 90% for the frequency range above 50 GHz. The bottom panel of Figure 7 shows differential transmittance, $T_e - T_o$.

V. DISCUSSIONS

A. Design shape V.S. Fabricated shape

There is a clear difference between the design shape and the fabricated shape when the laser machining is used. This is a unique feature due to the nature of the laser machining as compared to the mechanical machining. Figure 8 shows the comparison of two transmittances between one based on the design shape and one based on the fabricated shape. While the exact shape is not identical, the overall shape which is parametrized by the pitch, height, and top width are close to the design values and the resultant transmittance is qualitatively tracing well.

B. Optimization in shape

We investigate the design optimization in the detailed shape. The shape is parameterized as shown in Figure 9. In addition to the three parameters, the height, the pitch, and the top width, we also introduce the curvature (slope parameter, α) and the bottom width. The curvature is modelled as

$$w(z) = w_0 + \{(p - b) - w_0\} \left\{ 1 - \left(\frac{z}{h} \right)^\alpha \right\}.$$

Figure 9 shows the example of the three profiles for $\alpha = 0.5, 1, \text{ and } 1.5$. The profile with $\alpha = 1$ corresponds to the straight line.

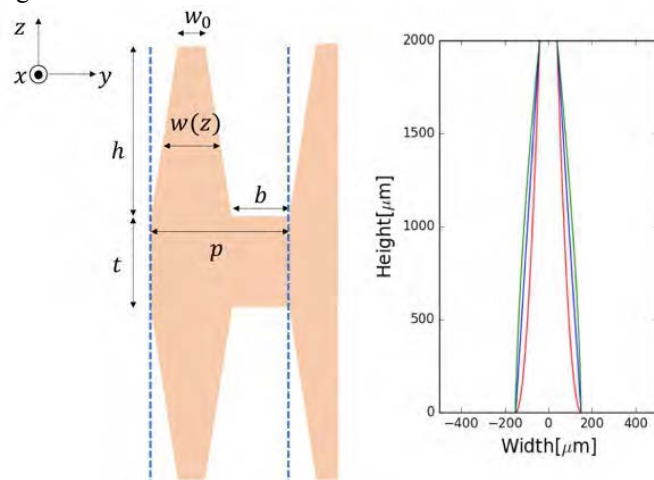


Figure 9 Left shows the parametrization for the optimization of the pyramidal shape. Right panel shows the pyramidal shape profile with the three different slope parameters, $\alpha = 0.5, 1, \text{ and } 1.5$.

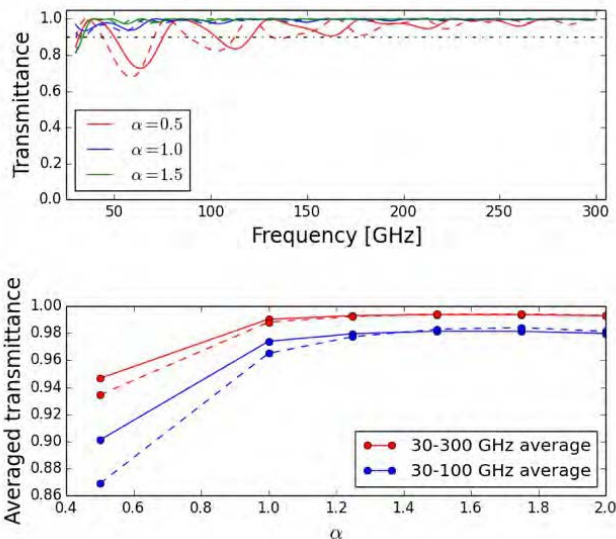


Figure 10 Top: Transmittance for the slope parameters, $\alpha = 0.5, 1, \text{ and } 1.5$.

Bottom: The band averaged transmittance for various slope parameters. For both plots, the solid line is Transmittance for n_o and the dashed line is for n_e .

We have studied the sensitivity of Transmittance to two parameters, the slope parameter, α , and the top width, w_0 . The top panel of the Figure 10 shows the difference of transmittance computed by RCWA for three different α values. The bottom panel of the Figure 10 shows the averaged transmittance between 30 and 300 GHz and also between 30 and 100 GHz as a function of the slope parameter, α . The profile with $\alpha > 1$ is more desirable to increase transmittance

at low frequency, $< \sim 100$ GHz, as compared to the case with $\alpha < 1$. However, the higher slope parameter eventually reaches to the limit which makes the pyramidal shape to be a rectangular. There is a wide range of an optical slope parameter ranges between 1 and 1.8. The top panel of Figure 11 shows transmittance for various values in the top width. The bottom panel of Figure 11 shows average transmittance as

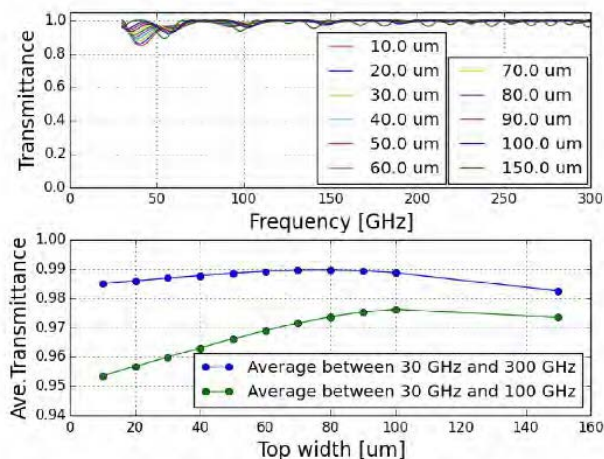


Figure 11 Top: Transmittance is plotted for various top width values. Bottom: Averaged transmittance as a function of the top width.

a function of the top width. We see the optimal top width to be around $80\text{--}100 \mu\text{m}$ depending on the bandwidth of interest. The fabricated sample is $w_0 = 51 \mu\text{m}$, and clearly there is a room for more improvement in transmittance particularly at low frequencies, below 100 GHz, by increasing the top width to be wider.

Based on this study, we explore further optimizations in the fabrication process toward the optimal shape. The laser machining contains various parameters to tune, including the laser pulse width, wavelength, energy, laser optical properties, and scan strategy. There is a huge parameter space to explore and it is beyond this paper to cover the entire optimization process. Yet, we shall describe one example of the fabricated shape which leads to higher transmittance in the low frequency range.

We have constructed a small prototype sample shown in Figure 12. We label this sample as a sample B. Figure 13 is transmittance that is computed by the DiffractMOD for the sample B assuming that this SWS is applied on the both surfaces of the sapphire plate. Clearly, transmittance from the sample B shows higher transmittance in the low frequency range, below 100 GHz, as compare to that from the sample A.

From the confocal microscope data, we can compute the area fraction of a material to the air region along the z -axis for both samples. Based on this data, we can compute the effective index of refraction at each slice in the z -axis using the second order EMT. The top and the bottom panels of Figure 14 show these relationships. We also over-plot the Klopfenstein profile as a reference [19,20], which is an optimal profile for a broadband AR coating particularly at the

low frequency side. Based on the study in Figure 10 and 11, transmittance in the low frequency region is higher for $\alpha > 1$ and $w_0 \sim 100 \mu\text{m}$. The shape of the sample B is closer match to these conditions as compared to that of the sample A.

C. Beyond transmittance

We started the development of the AR SWS with the design goal which is set by transmittance. High transmittance is very

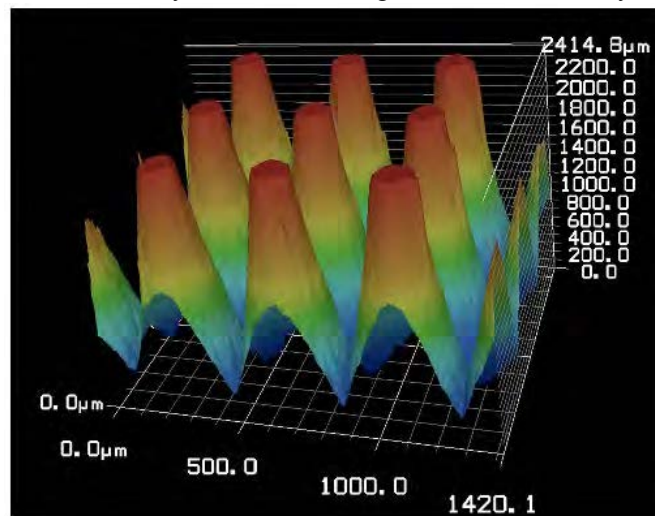


Figure 12 The confocal image of the sample B.

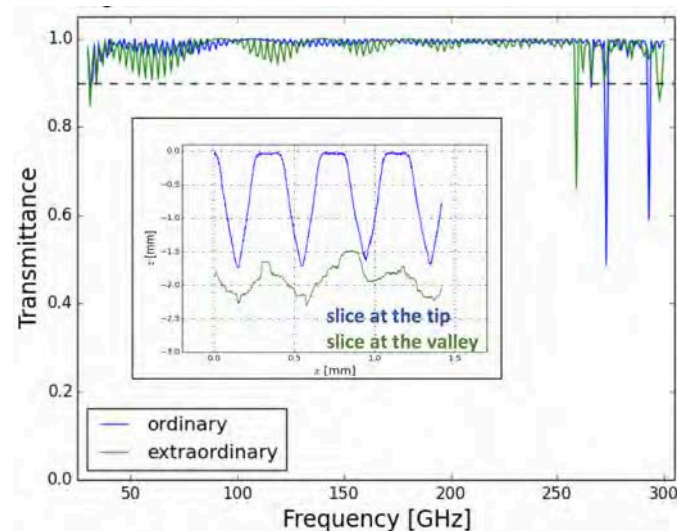


Figure 13 Projected transmittance of the sample B when the AR SWS is applied on the both surfaces of the sapphire plate. The inset shows the sliced shape profile at the tip and the valley.

important in the CMB polarization experiment. The reduction of the total signal power due to low transmittance degrades the signal-to-noise of the experiment and also becomes a source of a systematic effect, such as multiple reflections within a system.

When the AR coating is considered to a sapphire for use as a HWP, there are other parameters to be optimized. Transmittance along the ordinary and extra-ordinary axes results two different transmittances, T_o and T_e , due to the different indices of refraction. Differential transmission can be

a source of an instrumental systematic effect, and this is a secondary figure-of-metric to minimize. In our design, we did not take into account this effect, but we can include this in our design requirement.

Projected differential transmission based on the fabricated AR SWS has its own spectral signature as shown in the bottom panel of Figure 7. At the time of design, the modeled pyramidal shape was symmetric about the z -axis. In principle, we can increase the degree of freedom by introducing the

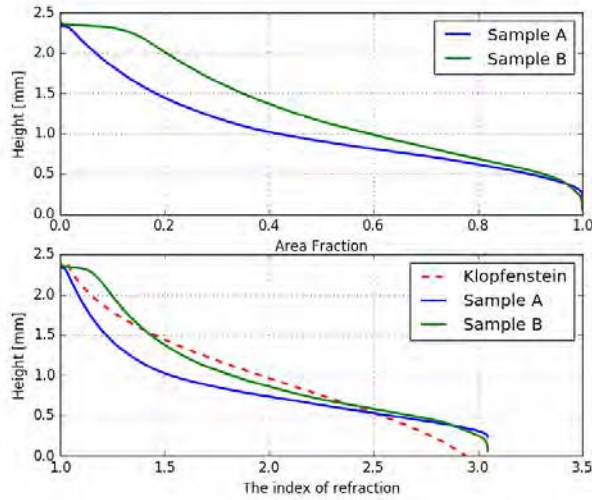


Figure 14 Top: The relationship between the height and the fractional area of the material at each slice along the z -axis. Bottom: The relationship between the height and the index profile which is estimated by the second order EMT.

asymmetry, e.g. rectangular base and top area with, p_x , p_y , and w_{0x} , w_{0y} . This allows the better impedance match for both the ordinary and extraordinary axes if the SWS is patterned with a proper alignment with the crystal axis.

CONCLUSIONS

We design the AR on sapphire using the SWS. We fabricate the SWS AR on one side of the C-cut sapphire prototype sample and measure transmittance. Measured transmittance and the predicted performance given the AR shape agree. Prospective transmittance when the AR SWS is applied on both surfaces is calculated. Prospective transmittance achieves above 90% for the frequency range above 70 GHz. When the band is averaged over 30% fractional bandwidth, the oscillatory feature is smeared and averaged transmittance achieves above 90% for the frequency range above 50 GHz. We also study the sensitivity of the AR design parameters and discuss the pros and cons for the further improvement in transmittance.

ACKNOWLEDGMENT

This work was supported by JSPS KAKENHI Grant Number 15H05441, 17H01125, 17K14272. This work was also supported by JSPS Core-to-Core Program, A. This work

was also supported by World Premier International Research Center Initiative (WPI), MEXT, Japan.

REFERENCES

- [1] Planck collaborations, "Planck 2015 results. I. Overview of products and scientific results", A&A 594, A1 (2016).
- [2] M. H. Abitbol et al., "CMB-S4 Technology Book, First Edition", arXiv:1706.02464.
- [3] E Hecht, "Optics", Addison-Wesley.
- [4] D. Rosen et al., "Epoxy-based broadband antireflection coating for millimeter-wave optics," Appl. Opt. 52, 8102–8105 (2013).
- [5] Y. Inoue et al., "Cryogenic infrared filter made of alumina for use at millimeter wavelength". Appl. Opt., 53(9):1727–1733, Mar 2014.
- [6] O. Jeong, A. Lee, C. Raum, and A. Suzuki, "Broadband plasma-sprayed anti-reflection coating for millimeter-wave astrophysics experiments", Journal of Low Temperature Physics, pages 1–6, 2016.
- [7] R. Datta, C. D. Munson, M. D. Niemack, J. J. McMahon, J. Britton, E. J. Wollack, J. Beall, M. J. Devlin, J. Fowler, P. Gallardo, J. Hubmayr, K. Irwin, L. Newburgh, J. P. Nibarger, L. Page, M. A. Quijada, B. L. Schmitt, S. T. Staggs, R. Thornton, and L. Zhang, "Large aperture wide-bandwidth antireflection-coated silicon lenses for millimeter wavelengths", Appl. Opt., 52(36):8747–8758, Dec 2013.
- [8] T. Matsumura, K. Young, Q. Wen, S. Hanany, H. Ishino, Y. Inoue, M. Hazumi, J. Koch, O. Suttman, and V. Schuetz, "Millimeter-wave broadband antireflection coatings using laser ablation of subwavelength structures", Applied Optics, 55:3502, May 2016.
- [9] Karl Young, Qi Wen, Shaul Hanany, Hiroaki Imada, Jürgen Koch, Tomotake Matsumura, Oliver Suttman, and Viktor Schütz., "Broadband millimeter-wave anti-reflection coatings on silicon using pyramidal sub-wavelength structures", Journal of Applied Physics 121, 213103 (2017).
- [10] Viktor Schütz, Karl Young, Tomotake Matsumura, Shaul Hanany, Jürgen Koch, Oliver Suttman, Ludger Overmeyer, and Qi Wen, "Laser Processing of Sub-Wavelength Structures on Sapphire and Alumina for Millimeter Wavelength Broadband Anti-Reflection Coatings", JLMN-Journal of Laser Micro/Nanoengineering Vol. 11, No. 2, 2016.
- [11] Fabien Defrance, Cecile Jung-Kubiak, Jack Sayers, Jake Connors, Clare deYoung, Matthew I. Hollister, Hiroshige Yoshida, Goutam Chattopadhyay, Sunil R. Golwala, and Simon J. E. Radford, "1.6:1 bandwidth two-layer antireflection structure for silicon matched to the 190–310 GHz atmospheric window", Applied Optics Vol. 57, Issue 18, pp. 5196-5209 (2018).
- [12] Patricio A. Gallardo, Brian J. Koopman, Nicholas F. Cothard, Sarah Marie M. Bruno, German Cortes-Medellin, Galen Marchetti, Kevin H. Miller, Brenna Mockler, Michael D. Niemack, Gordon Stacey, and Edward J. Wollack, "Deep reactive ion etched anti-reflection coatings for sub-millimeter silicon optics", Applied Optics Vol. 56, Issue 10, pp. 2796-2803 (2017).
- [13] Ishino et al., "LiteBIRD: lite satellite for the study of B-mode polarization and inflation from cosmic microwave background radiation detection", Proceedings Volume 9904, Space Telescopes and Instrumentation 2016: Optical, Infrared, and Millimeter Wave; 99040X (2016); doi: 10.1117/12.2231995.
- [14] Y. Sekimoto et al., "Concept design of the LiteBIRD satellite for CMB B-mode polarization", submitted to SPIE conference proceedings (2018).
- [15] R. Bräuer et al., "Design of antireflection gratings with approximate and rigorous methods," Appl. Opt. 33, 7875–7882 (1994).
- [16] DiffractMOD from RSoft/Synopsys.
- [17] B. R. Johnson, "MAXIPOL: A bolometric, balloon-borne experiment for measuring the polarization anisotropy of the cosmic microwave background radiation", Ph.D. thesis, University of Minnesota.
- [18] K. Komatsu et al., "Prototype design and evaluation of the 9 layer achromatic half-wave plate for LiteBIRD low frequency telescope", submitted to the SPIE proceedings 2018.
- [19] R. W. Klopfenstein, "A transmission line taper of improved design", Proceedings of the IRE (Volume: 44, Issue: 1, Jan. 1956).
- [20] E. B. Grann et al., "Optimal design for antireflective tapered two-dimensional subwavelength grating structures", Vol. 12, No. 2/February 1995/J. Opt. Soc. Am. A.